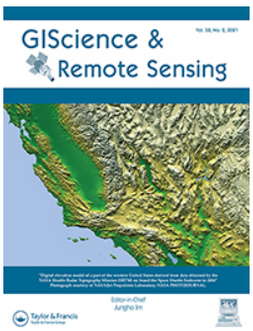

GIScience & Remote Sensing

ISSN: (Print) (Online) Journal homepage: https://www.tandfonline.com/loi/tgrs20

Effect of landscape pattern and spatial configuration of vegetation patches on urban warming and cooling in Harare metropolitan city, Zimbabwe

Pedzisai Kowe, Onisimo Mutanga, John Odindi & Timothy Dube

To cite this article: Pedzisai Kowe, Onisimo Mutanga, John Odindi & Timothy Dube (2021) Effect of landscape pattern and spatial configuration of vegetation patches on urban warming and cooling in Harare metropolitan city, Zimbabwe, GIScience & Remote Sensing, 58:2, 261-280, DOI: 10.1080/15481603.2021.1877008

To link to this article: https://doi.org/10.1080/15481603.2021.1877008

Published online: 07 Feb 2021.

GISCIENCE & REMOTE SENSING
2021, VOL. 58, NO. 2, 261–280
https://doi.org/10.1080/15481603.2021.1877008

Taylor & Francis
Taylor & Francis Group

ARTICLE

Effect of landscape pattern and spatial configuration of vegetation patches on urban warming and cooling in Harare metropolitan city, Zimbabwe

Pedzisai Kowe[a,b], Onisimo Mutanga[a], John Odindi[a] and Timothy Dube[c]

[a]Discipline of Geography, School of Agricultural, Earth and Environmental Sciences, University of KwaZulu-Natal, Private Bag X01, Pietermaritzburg, South Africa; [b]Scientific and Industrial Research and Development Centre (SIRDC), Geo-Information and Remote Sensing Institute, Harare, Zimbabwe; [c]Department of Earth Sciences, University of the Western Cape, Bellville, South Africa

ABSTRACT

The spatial configuration of vegetation patches in the landscape has implications for the provision of ecosystem services, human adaptation to climate change, enhancement, or mitigation of urban heat island. Until recently, the effect of spatial configuration of vegetation to enhance or mitigate urban heat island has received little consideration in urban thermal assessments. This study examines the impact of spatial configuration of vegetation patches on urban thermal warming and cooling in Harare metropolitan city, Zimbabwe. The study used Advanced Spaceborne Thermal Emission and Reflection Radiometer (ASTER), Landsat and Sentinel 2 data acquired between 1994 and 2017 to derive detailed information on vegetation patches, landscape metrics, and land surface temperature LST(°C). The spatial configuration of urban vegetation patterns was analyzed using landscape metrics in Fragstats program. Getis Ord Gi* as a Local Indicator of Spatial Association (LISA) was used to characterize the spatial clustering and dispersion of urban vegetation patches. Results of the Getis Ord Gi* showed that clustered vegetation lowers surface temperatures more effectively than dispersed and fragmented patterns of vegetation. The size, density, shape complexity, and cohesion of vegetation patches conferred different levels of cooling but Patch Cohesion Index had the strongest negative relationship with LST(°C) at three spatial resolutions of 10 m (Sentinel 2), 15 m (ASTER) and 30 m (Landsat 8). The Spatial Lag Regression model performed better than the Ordinary Least Squares regression analysis in exploring the relationship between LST(°C) and landscape metrics. Specifically, the Spatial Lag Regression model showed higher R^2 values and log likelihood, lower Schwarz criteria, and Akaike information criterion, and reduced spatial autocorrelations. The overall information provides important insights into the provision of larger, connected, and less fragmented urban vegetation patches to derive maximum and higher cooling effects which is critical for urban planning and design approaches for mitigating increasing surface temperatures in cities.

ARTICLE HISTORY
Received 14 June 2019
Accepted 10 January 2021

KEYWORDS
Urban Heat Island; urban warming and cooling; land surface temperature; vegetation; landscape metrics; Harare

1.0 Introduction and background

With increasing global urbanization, climate change and global warming, urban heat island (UHI) effects (Oke 1982; Voogt and Oke 2003) are expected to grow in intensity (Gabriel and Endlicher 2011; Gill et al. 2007; Wang and Akbari 2016). Urban heat island effects cause higher temperatures and increase the number of warm nights in urban areas than in less developed, rural, and surrounding areas (Oke 1982). Urban warmth and high surface temperatures reduce annual energy consumption in cold climates (Svensson and Eliasson 2002), but the reverse is true in warm and tropical cities where summer air conditioning demand loads far outweigh potential savings in energy use for heating during winter (Santamouris et al. 2001). Intensified UHI can lead to increased demands for water consumption (Guhathakurta and Gober 2007), elevated concentration of air pollutants (Lai and Cheng 2009), and degraded water quality (Arnold and Gibbons 1996). UHI worsens the thermal comfort conditions, heat-related health problems, and welfare of urban dwellers (Tomlinson et al. 2011). The urban climate is likely to become more uncomfortable, especially in summer, when heat released from the urban infrastructure at night increases the duration and intensity of heat waves (Tomlinson et al. 2011).

Urban green spaces (UGSs) and vegetation cover including urban parks, street trees, lawns, woodlands, forests, grasslands, playgrounds, and green belts are considered to be important components of urban climate (Dobbs, Nitschke, and Kendal 2014; Gill et al.

CONTACT Pedzisai Kowe Kowemuso5@gmail.com

2007) in mitigating the effects of UHI. For instance, Kong et al (2014a) observed a reduction of land surface temperature (LST°C) by 0.83°C in the city of Nanjing in China following a 10% increase in forest and green spaces. This is due to the fact that evapotranspiration and shading from trees and green spaces within urban areas reduce surface temperatures, which may subsequently reduce the amount of energy needed to cool buildings. The positive role of urban green spaces and vegetation cover in mitigating urban thermal islands is already established through measurements (field measurements, models, and thermal remote sensing of land surface temperature) and computer simulation (Farhadi, Faizi, and Sanaieian 2019; Lai et al. 2019). The majority of scholarly work studying the effect of spatial arrangement patterns of urban green spaces (UGSs) and vegetation cover on UHI have been conducted over the past 10 years (Aram et al. 2019).

However, current knowledge on the effects of urban vegetation and green spaces on LST(°C) is not comprehensive as it ignores the possible influence of landscape pattern and spatial configuration of vegetation patches such as edge density, shape complexity, size, aggregation, connectivity, and fragmentation on their cooling effect (Masoudi, Tan, and Liew 2019). The results of a relatively small but growing number of research studies indicate that the landscape pattern and spatial configuration of urban vegetation patches has significant impacts on LST(°C) and can be optimized to mitigate the UHI effect (Asgarian, Amiri, and Sakieh 2015; Bao et al. 2016; Chen et al. 2014; Connors, Galletti, and Chow 2013; Estoque, Murayama, and Myint 2017; Huang and Cadenasso 2016, Kong et al. 2014a; Li et al. 2012, 2016, 2017; Maimaitiyiming et al. 2014; Zhang et al. 2009; Zhibin et al. 2015; Zhou, Huang, and Cadenasso 2011). For instance, urban green spaces and vegetation patches with more complex shapes were shown to deliver higher cooling effects (Asgarian, Amiri, and Sakieh 2015; Chen et al. 2014; Estoque, Murayama, and Myint 2017; Li et al. 2012; Zhang et al. 2009; Zhou, Huang, and Cadenasso 2011). Other studies have shown that the size of urban green space is responsible for higher cooling effects (Feyisa, Dons, and Meilby 2014; Hamada, Tanaka, and Ohta 2013).

Even though the spatial configuration is strongly affected by ecological processes based on the concept of landscape ecology, it should be noted that not all landscape metrics of landscape configuration are responsible for the thermal processes in city or urban area (Chen et al. 2016). In addition, most landscape metrics are highly correlated with each other and create serious challenges with redundancy and difficulty in interpretation (Song et al. 2014; Uuemaa, Mander, and Marja 2013). For instance, some uncertainties and inconsistencies exist regarding the effects of other spatial configuration patterns such as connectivity and aggregation of vegetation patches on the resultant cooling and warming of the urban environment. For instance, the positive effects of spatial patterns of connectivity and aggregation of urban green spaces (UGSs) and vegetation patches have been observed in some studies (Asgarian, Amiri, and Sakieh 2015; Chen et al. 2014; Estoque, Murayama, and Myint 2017), whereas in other studies (Bao et al. 2016; Chen et al. 2014a, Li et al. 2012; Li, Zhou, and Ouyang 2013; Zhou, Huang, and Cadenasso 2011), the opposite has been reported. Therefore, appropriate selection of landscape metrics in relation to thermal processes is important capturing the effects of landscape configuration on any variation in LST(°C) (Chen et al. 2016).

Furthermore, most of these landscape metrics do fully represent the dispersed and clustered spatial patterns of each land cover category, because they are calculated based upon discrete maps and ignore all other variation (Fan and Myint 2014; Myint et al. 2015; McGarigal and Cushman 2005; McGarigal, Tagil, and Cushman 2009). Consequently, most UHI studies do not consider spatial configurations as continuous surfaces but rather as discrete spatial variation resulting in loss of vital information (Myint et al. 2015). The ultimate result has been that effects of spatial autocorrelation of LST(°C) are not taken into account in most existing UHI studies (Chen et al. 2006; Li et al. 2011; Zhou, Huang, and Cadenasso 2011) when performing conventional and regression analysis of the relationships between LST(°C) and landscape indices.

In order to address the limitations associated with discrete landscape metrics, an alternative and effective approach is to use continuous methods of local spatial autocorrelation indices, also known as Local Indicator of Spatial Association (LISA) (Anselin 1995). Previous studies have indicated that the local Moran's I index (Anselin 1995) to be very effective in characterizing the impact of clustered and dispersed spatial configurations and composition patterns of

vegetation cover (Fan, Myint, and Zheng 2015), impervious surface area (Wu et al. 2019) and other land cover categories (Myint et al. 2015; Zheng, Myint, and Fan 2014) on surface temperatures. Unlike local Moran's I index, the utility of Getis-Ord Gi* has largely been ignored in examining the impact of clustered and dispersed spatial configurations of vegetation on UHI studies. Only recent applications of Getis-Ord Gi statistics in UHI studies, have analyzed the LST pattern change through time to assess the impacts of land use/land cover change and urbanization on UHI (Tran et al. 2017) and to identify the high concentration of the LST visually across an urban landscape (Adeyeri, Akinsanola, and Ishola 2017; Tran et al. 2017).

Furthermore, it is not known how sensitive are findings of LST(°C) to the spatial resolution of the underlying data relative to the grain size of heterogeneity of urban vegetation and land cover. Previous studies have mainly examined these relationships for a single scale, which is usually the spatial resolution of satellite imagery data from which landscape metrics and LST(°C) are derived. The issue of spatial resolution is relevant where landscape metrics are scale-dependent on the spatial resolution of the remote sensing and other data sources as they change with the scale of the observation or analysis (Turner 1989; Wu et al. 2000, 2002) as well as their relationships with LST(°C) (Kong et al. 2014b; Li, Zhou, and Ouyang 2013; Song et al. 2014). The landscape patterns of green spaces have ecological implications at varying spatial resolution and scales. It could produce different amounts of latent heat of evapotranspiration which in turn influences the distribution of habitat and material energy fluxes in the landscape, thus resulting in diverse thermal effects (Adams and Smith 2014; Berger et al. 2017; Chen et al. 2017; Forman 1995; Turner 2005; Zhou et al. 2014).

However, to date, spatial configuration studies have largely been conducted mainly in cities of United States of America (Buyantuyev and Wu 2010; Maimaitiyiming et al. 2014; Myint 2012; Myint et al. 2013, 2015) and China (Kong et al. 2014a; Kong et al. 2014b; Li et al. 2012; Zhang et al. 2009; Zhang, Lv, and Pan 2013). Cities from Africa are largely ignored. The conclusions and implications drawn from these studies may not be comprehensive because of the limitations of the geographical locations, regional climate conditions, and different patterns of urban and economic growth levels. Given this background, the objective of this study was to examine how landscape pattern and spatial configuration of urban vegetation significantly enhance or mitigate the urban warming in the Harare metropolitan city, Zimbabwe. The study further examined the effects and sensitivity of the spatial resolution on the relationship between LST(°C) and the spatial configuration of vegetation by using multi-regression models after controlling spatial autocorrelation effects. This paper is organized in the sections. Following the description of the study area, the methodology of calculating LST(°C), landscape metrics, Getis-Ord Gi*, spatial regression models is presented in Section 2. The results, discussions and conclusions and recommendations are presented in Section 3,4 and 5, respectively.

2.0 Materials and methods

2.1 Study area

This study was conducted in Harare metropolitan city, which is located in the north-eastern part of Zimbabwe. The Harare metropolitan city encompasses Harare urban and rural, satellite towns of Epworth and Ruwa to the east and Chitungwiza to the south (ZIMSTAT 2012). Harare is the economic hub, administrative capital and the largest city of Zimbabwe. The population of Harare in the year 2012 was 2.1 million (ZIMSTAT 2012). (Figure 1) shows the location of Harare metropolitan city. It is situated at 17.83° latitude and 31.05°longitude. The city has an area of approximately 980.6 square kilometers. Harare metropolitan city is characterized by a mainly flat topography in the southern part and is generally hilly in the northern part. The city falls within the subtropical highland climate, which are mild and cool with relatively longer sunshine hours. It experiences warm summers (average temperature 26°C) and cold winters (average temperature 10°C).

The western, southern, and eastern parts portion of the Harare metropolitan city is largely composed of urban and built-up areas with dominance of high-density residential areas. The northern portion is largely vegetated with predominance of low-density residential areas. Despite being a highly built-up and urbanized city, there are also protected forest and vegetated areas in Harare, which includes Haka game park (Cleveland dam vegetation), Mukuvisi

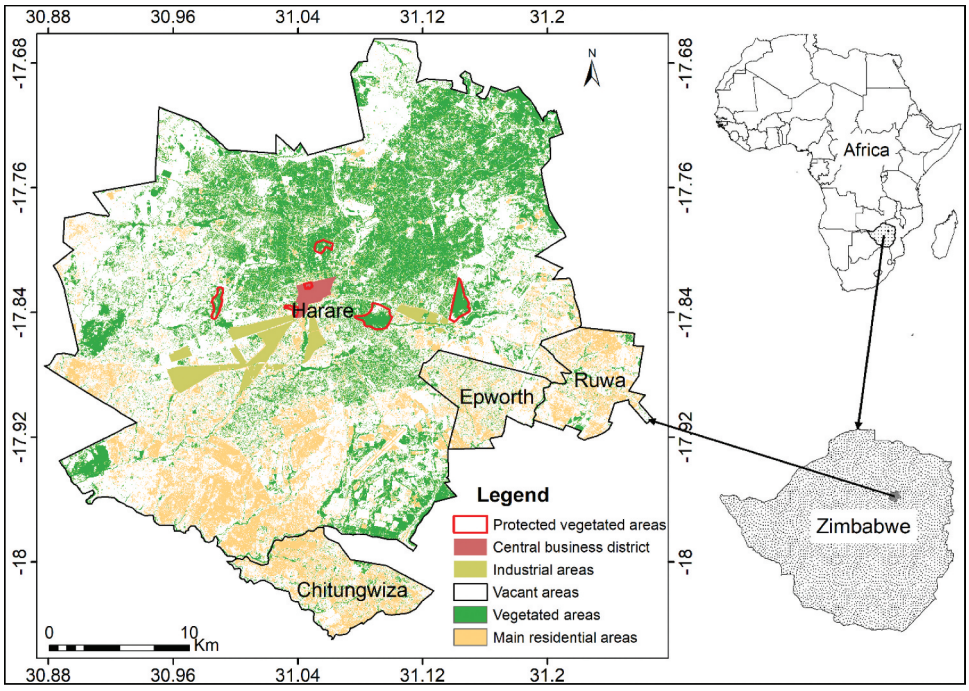

Figure 1. The geographical location of the study area, Harare metropolitan city in Zimbabwe.

woodlands, Harare Kopje, Harare botanical gardens, and the vegetation surrounding the Harare National Heroes Acre.

Harare metropolitan city was selected for this study because it has witnessed a rapid urbanization process over the past few decades (Kamusoko, Gamba, and Murakami 2013) and the trend is expected to continue (Mushore et al. 2017) mostly replacing open spaces and surrounding natural habitats (grassland and remnant forests). Such a rapid urbanization also inevitably generates urban heat island effect because of the increasing built-up developments, loss of vegetation, and increase in land surface temperature. Given the continued urban expansion of the Harare metropolitan city, a better understanding of the relationship between the spatial configuration of urban vegetation cover and LST(°C) can provide significant insights for the energy balance, ecological functioning of the city, sustainable urban management, and the mitigation of urban heat island.

2.2. Satellite data

This section outlines the various satellite datasets used in this study and are summarized in (Table 1). The data used in this study consist of six satellite images, an Advanced Spaceborne Thermal Emission and Reflection Radiometer (ASTER), a Sentinel 2 Multispectral Instrument (MSI) and four Landsat data (Table 1). Only ASTER imagery was acquired in September rather than in October due to cloud coverage challenges. The satellite imagery data were freely downloaded from Earth Explorer United States Geological Survey website (http://earthexplorer.usgs.gov/). The satellite data were in dry season because the images were cloud free and with more stable atmospheric factors. Dates of imagery were paired relatively close in time to help ensure consistency in land cover classification and phenology.

Table 1. Satellite image data.

Satellite data	Spatial resolution (m)	Date of Acquisition
Landsat 5	30 m(VNIR) and 120 (TIR)	8 October 1994
Landsat 7	30 m(VNIR) and 60 m (TIR)	19 October 2001
ASTER	15 m(VNIR) and 90 m (TIR)	3 September 2010
Landsat 8	30 m(VNIR) and 100 m (TIR)	28 October 2013
Sentinel 2	10 m (VNIR)	24 October 2017
Landsat 8	30 m(VNIR) and 100 m (TIR)	23 October 2017

Visible and Near Infrared (VNIR), and the Thermal Infrared (TIR)

The satellite datasets were used to derive detailed urban green and vegetation areas, landscape metrics and summer daytime land surface temperature data. Land surface temperature LST(°C) is one of the indicators of surface-energy balance (Voogt and Oke 2003) which is sensitive to surface characteristics.

Land surface temperature (LST°C) patterns derived from the thermal-infrared remote sensing imagery has been instrumental in capturing urban heat island effects (Weng, Lu, and Schubring 2004). Thermal data generally have coarser spatial resolution than shorter wavelength bands, placing further limitations on UHI studies. For example, the resolution of Landsat and ASTER's thermal bands are 60 m −100 m and 90 m, respectively, despite both having resolutions of 30 and 15 m for other bands. While Airborne sensors like Airborne Topographic Laser System (ATLAS) and Airborne Hyperspectral Scanner (AHS) can offer greater spatial and thermal resolution, airborne data are however, only available for small areas and at significant cost to the end user compared to that of moderate resolution sensors.

Similarly, this study did not use high-resolution data from commercial satellites as these are generally not as widely accessible for researchers and most of them do not have thermal bands. Although low and coarse resolution data like Moderate Resolution Imaging Spectroradiometer (MODIS) on the Terra and Aqua satellites and Advanced Very High Resolution Radiometer (AVHRR) are readily available, they have limitations in solving the problems of mixed pixels in heterogeneous urban areas. Low-resolution satellite images like MODIS and AVHRR are useful only for coarse-scale urban landscape mapping.

2.3 Urban green areas and vegetation extraction

The satellite data used in this study were initially classified into five land cover categories (i.e., vegetation, grassland, built-up, water, and bareland) with the supervised image classification approach using the support vector machine algorithm in the Environment for Visualizing Images (ENVI) 5.3 software image processing software. Later, the classified land cover map was reclassified into a binary vegetation and non-vegetation map for subsequent landscape analysis. A value of one and zero was assigned to vegetation and non-vegetation pixels, respectively. Vegetation consisted of forests, woodlands, shrubland, cropland, park and green land, and street trees, which are sometimes referred to as green spaces. The non-vegetation consisted of impervious surfaces, artificial structures including pavements and built-up areas, transportation, industrial, commercial and residential space, water, and bareland.

An accuracy assessment was conducted based on ground reference data derived from air photographs of 1994 and 2001, Google imagery of 2010 (ASTER), 2013 (Landsat 8), and 2017 (Sentinel 2 and Landsat 8). The overall accuracy of the error matrix was computed by dividing the total number of correctly classified pixels (sum along the major diagonal) by the total number of validation plots, known as percentage correct (Congalton and Green 1999). A non-parametric Kappa test was used to measure the land cover classification accuracy as it accounts for all the elements in the confusion matrix rather than the diagonal elements. The Kappa coefficient were calculated following the procedure given by Congalton and Green (1999).

2.4 Spatial configuration analysis of urban green vegetation

Since most landscape metrics are often correlated with one another and they should be relatively independent of each other with minimal redundancy, we only selected a suite of landscape metrics based on their widespread use in landscape analysis, their easy interpretation, and their relevance as indicators of ecosystem functioning (McGarigal 2002; Wu 2004; Riitters et al. 1995). After computing several landscape metrics, only five landscape metrics indices including Edge density (ED), Mean Patch Size (MPS), Area Weighted Mean Shape Index (AWMSI), Area Weighted Mean Patch Fractal Dimension (AWMPFD), and Patch Cohesion Index (Table 2) were further used in this study. The selected landscape metrics indices accounted for different and important dimensions of the landscape patterns and configurations of size,

Table 2. Description of landscape metrics used in the study area.

Landscape metrics	Description
Mean Patch Size/Area	The average mean surface of patches
Area-Weighted Mean Shape Index	A larger value of SHAPE_AM means the area is more complex and irregular in shape
Area-Weighted Mean Fractal Dimension Index	Fractal dimension: ratio of perimeter per unit area. Increases as patches become more irregular
Patch Cohesion Index	Increases as the patches of the corresponding patch type become less connected.
Edge Density	Total length of all edge segments in the landscape (green space) per hectare (m/ha)

density, shape, isolation, and connectivity of urban vegetation patches. The selected landscape metrics were computed from the binary vegetation and non-vegetation data. The landscape metrics were calculated using FRAGSTATS 4.2 software (McGarigal and Marks 1995; McGarigal 2002).

For the landscape metrics used, the lower Mean Patch Size values are usually associated with a more fragmented land cover pattern in a landscape. AWMSI and AWMPFDI are simple measures of patch shape complexity, in which the greater the value, the more complex and irregular the shape. The Patch Cohesion Index assesses the contiguity of the shape and the percentage of physically connected patches. Patch Cohesion index (COHESION) varies between 0 and 100%. A higher value of Patch Cohesion Index represents more physically connected patterns of patches in a landscape and vice versa (McGarigal 2002). A more detailed description for each landscape metric can be found in (McGarigal 2002).

2.5. Land surface temperature

The digital number(DN) of the thermal bands were first converted to spectral radiance (w/m^2/sr/μm) or Top of Atmosphere (TOA) reflectance according to radiometric rescaling coefficients (Chander and Markham 2003; Chander, Markham, and Helder 2009). Next, the spectral radiance was then converted to brightness temperature (i.e., blackbody temperature) in Kelvin at the sensor by applying the inverse of the Planck radiance function for temperature using the following formula.

$$T_B = \frac{K_2}{\ln\left(\left(\frac{K_1}{L_\lambda}\right)+1\right)} \quad (1)$$

where T_B is the at-sensor brightness temperature in degrees Kelvin.L_λ is spectral radiance in $Wm^{-2}sr^{-1}mm^{-1}$. $K_1$and $K_2$are calibration constant 1 and 2, respectively. For Landsat 5 (Band 6), the K_1 value is 607.76 and the K_2 value is 1260.56. On the other hand, Landsat 7 the thermal band 6's K_1 and the K_2 values are 666.09 and is 1282.71, respectively. For Landsat 8 Band 10, the K_1 value is 774.89 and the K_2 value is 1321.08, respectively. For Aster band 13, the K_1 value is 866.46 and the K_2 value is 1350.06, respectively.

This process is followed by a correction for land surface emissivity (**ε**) according to the nature of the landscape (Sobrino, Jiménez-Muñoz, and Paolini 2004). The land surface emissivity (**ε**) values ranges between 0.97 and 0.99. The land surface emissivity (**ε**) was assigned to be 0.97 at NDVI < 0.2 and 0.99 at NDVI > 0.5 using the NDVI thresholds method proposed by Sobrino, Jiménez-Muñoz, and Paolini (2004). When 0.2 ≤ NDV I ≤ 0.5, the emissivity was calculated by the following formula:

$$\varepsilon = 0.004 * P_v + 0.986 \quad (2)$$

where P_v is the Proportion of Vegetation(Carlson and Ripley 1997; Sobrino, Jiménez-Muñoz, and Paolini 2004). The Proportion of Vegetation (Pv) of each pixel was determined from the NDVI using the following equation (Carlson and Ripley 1997)

$$P_v = \left(\frac{NDVI - NDVI_{min}}{NDVI_{max} - NDVI_{min}}\right)2 \quad (3)$$

where $NDVI_{min}$ is the minimum NDVI value (0.2) where pixels are considered as bare soil (non-vegetated areas) and $NDVI_{max}$ is the maximum NDVI value (0.5) where pixels are considered as healthy vegetation and dense vegetation. The Normalized Difference Vegetation Index (NDVI) (Tucker 1979) which is an index of living green vegetation, was derived from Aster and Landsat 8 satellite data by using the following equation:

$$NDVI = \left(\frac{NIR - R}{NIR + R}\right) \quad (4)$$

Where R and NIR are the red and infrared bands, respectively, as derived from image data.

Lastly, the emissivity-corrected LST(°C) was computed using the following equation (Weng, Lu, and Schubring 2004; Sobrino, Jiménez-Muñoz, and Paolini 2004)

$$\mathrm{LST} = \left[\frac{T_B}{1 + (\lambda\sigma T_B/(hc))\ln\varepsilon}\right] - 273.15 \quad (5)$$

where LST = land surface temperature, T_B = at-satellite brightness temperature, λ = wavelength of emitted radiance (λ = 10.8 μm for Landsat 8 Thermal Infrared Sensor (TIRS) (Band 10), σ is Boltzmann constant (1.38×10^{-23}J/K), h =Planck's constant(6.626×10^{-34}Js), c =velocity of light (2.998×10^{-8}m/s). The retrieved LST(°C) values were later converted from degrees Kelvin to degrees Celsius (°C) by subtracting 273.15

from the calculated pixel values. An absolute zero, 0°C equals 273.15 Kelvin (K).

2.6 Spatial clustering and dispersion of vegetation based on getis-ord gi*

Based on NDVI(Tucker 1979) data, Getis-Ord Gi* as a local indicator of spatial association (LISA) (Anselin 1995), known also as hot-spot analysis (Getis and Ord 1992; Ord and Getis 1995) was calculated in ENVI image processing software to map the spatial clustering and dispersion of vegetation patterns in the study area. This technique characterizes the presence of hot spots (high clustered values) and cold spots (low clustered values) over an entire area by looking at each feature within the context of its neighboring features (Ord and Getis 1995). The Getis-Ord Gi* statistic was calculated according to (Getis and Ord 1992).

$$G_i^*(d) = \frac{\sum_{j=1}^{n} w_{ij}(d)x_j - W_i^*\bar{x}}{s\left[W_i^*\left(n - W_i^*\right)/(n-1)^{1/2}\right]} \quad (7)$$

$\bar{x}$ and s are mean and standard deviation, respectively. Basically, wij is calculated on the basis of the conceptualized spatial relationship and in reference to d. Therefore, it is often written as wij(d). Following the methodology of Myint et al. (2015), Getis-Ord Gi* values were normalized to the range of −1 to 1. Positive values of Getis-Ord Gi* statistic represent highly clustered and homogeneous patterns that are, on average, greater than the mean. Getis-Ord Gi* of negative values represent highly dispersed and heterogeneous patterns that are less than the mean. Values of zero indicate random patterns with no apparent spatial clustering. Getis-Ord Gi* statistic is effective in rainfall modeling (Liu et al. 2019), crime analysis (Craglia, Haining, and Wiles 2000), incident management (Songchitruksa and Zeng 2010), heat vulnerability assessment (Wolf and McGregor 2013) as well as in agriculture (Chopin and Blazy 2013; Rud, Shoshany, and Alchanatis 2013).

2.7 Statistical analysis

Pearson's product-moment correlation coefficient was computed to evaluate the relationship between LST(°C) and the selected landscape metrics of vegetation or green space. LST(°C) was the dependent variable in our analysis and landscape metrics of Edge density (ED), Mean Patch Size (MPS), Area-Weighted Mean Shape Index (AWMSI), Area-Weighted Mean Patch Fractal Dimension (AWMPFD) and Patch Cohesion Index were the independent variables. A negative correlation means a reducing effect on LST(°C) and a positive correlation means that the landscape pattern component can increase and enhance LST(°C). The landscape metrics of vegetation derived from ASTER image and Landsat 5, 7, and 8 were related to the LST(°C) of the same images, respectively. Since Sentinel 2 does not have thermal bands, the landscape metrics of vegetation derived from Sentinel 2 of 2017 were compared to the LST(°C) acquired from Landsat 8 Thermal Infrared Sensor (TIRS) of 2017.

2.8. Spatial autocorrelation of LST(°C)

This section will introduce the concepts of spatial regression analysis and spatial autocorrelation. The Global Moran's I index (Moran 1950; Cliff and Ord 1981; Legendre and Fortin 1989) was used to measure the spatial autocorrelation of LST(°C) for the ASTER acquired on September 9, 2010 and on the Landsat 5 acquired on October 8, 1994, Landsat 7 acquired on October 19, 2001 and Landsat 8 acquired on October 23, 2017. Moran's I is the most common method to describe the degree of spatial concentration or dispersion for the variables and their proximity in geographical space which is defined as follows;

$$Moran's\ I = \frac{n\sum_i\sum_j w_{ij}(d)(x_i - \bar{x})(x_i - \bar{x})}{\sum_i\sum_j w_{ij}\sum_i (x_{i-}\bar{x})^2} \quad (8)$$

i and j depict the various locations, xi and xj are the values of the variable x of location i and j, respectively, $\bar{x}$ is the mean value of the variable and w_{ij} represents a spatial weight matrix for measuring spatial proximity(connectivity) between i and j locations. The Moran's 1 is standardized and Moran's I values range from−1 to 1, hence positive Moran's I index values indicates a tendency toward spatial clustering (0 to ≥ 1) and more significant spatial autocorrelation. The negative Moran's I index values indicates a tendency toward spatial dispersion (0 to ≥ −1) and zero suggests that there is no spatial autocorrelation.

The Global Moran's I was conducted using a queen contiguity matrix to create the spatial weights matrix

defining the neighboring size of LST(°C). The queen contiguity weights criterion is recommended in practice to deal with potential inaccuracies in the polygon file (such as rounding errors) (Anselin 2003). A significant spatial autocorrelation ($p < 0.05$) was detected in LST(°C) data violating the critical assumption of sample independence required by parametric tests. After discovering significant spatial autocorrelation, we therefore used the Lagrange Multiplier test in the Geoda software package (Anselin 2003, Anselin 2006) to determine the more appropriate spatial autoregression models specifications: either the spatial lag or spatial error that integrate spatial autocorrelation. One of the critical outcomes of this study is that the inclusion of any of the spatial autoregression model (spatial lag or spatial error) into examining the relationships between LST(°C) and spatial configuration patterns of vegetation results in a decrease in the Akaike Information Criterion (AIC), as can be seen when comparing the Ordinary Least Squares (OLS) and spatial lag models.

2.9 OLS and SLM models analysis

Two regression models, the Ordinary Least Squares (OLS) (Model 1) and a Spatial Lag model SLM (Model 2) were developed to predict the mean LST(°C) as the dependent variable. The selected landscape indices of Mean Patch Size, Area-Weighted Mean Patch Fractal Dimension Index, Area-Weighted Mean Shape Index, and Edge Density were independent variables at 10 m, 15 m, and 30 m spatial resolution. The Ordinary Least Squares (OLS) can be described as:

$$y = X\beta + \in \tag{9}$$

where y is the dependent variable, X is the matrix of explanatory variables without an intercept term; β is a vector of slopes; and ε is a vector of random error terms. In dealing with spatial data, the traditional regression model may not be appropriate resulting in a failure to capture the spatial dependence of data in the model residuals. Therefore, other spatial regression models including the spatial lag model (SLM) are often used. The spatial lag model (SLM) assume that the residuals could be the result of spatial autocorrelation in the dependent variable. The spatial lag model (SLM) is expressed as follows

$$y = \rho Wy + X\beta + \in \tag{10}$$

where ρ is a spatial autocorrelation parameter; and Wy is the spatial weight matrix.

The OLS and SLM regression models were compared to evaluate the performance and their goodness fit in explaining the relationship between LST(°C) and explanatory variables of landscape metrics. Four parameters including R^2, log likelihood, Akaike Information Criterion (AIC) and Schwarz criteria were selected to describe the fitness of the two models. The higher the R^2 value and the log likelihood of the model, the higher the model fitness. On the other hand, the lower the AIC and Schwarz criteria indicates better model fit. The analysis was conducted in the GeoDa software. (Figure 2) illustrate the research methodology undertaken in this study.

3.0 Results

3.1 Land cover classification accuracy and spatial pattern of vegetation in the city

The land cover classification for Harare metropolitan city of the six satellite imagery datasets had a high accuracy, which could be partly attributed to the simple classification scheme and the effectiveness of the robust support vector machine classification algorithm used. The overall accuracy of the land cover classification was 97.65% in 1994, 97.55% in 2001,96.12% in 2010, 96.13% in 2013. It was 97.14% and 97.32% for Landsat 8 acquired on 23 October 2017 and Sentinel 2 data acquired on October 24, 2017, respectively. On the other hand, the Kappa coefficient was 0.95 for ASTER data acquired on September 9, 2010 and Landsat 8 acquired on October 28, 2013, 0.96 for Landsat acquired in 1994, in 2001 both Landsat 8 acquired on October 23, 2017, and Sentinel 2 data acquired on October 24, 2017, respectively. This is more than 85%, the minimum level of mapping accuracy generally required for most land cover categories from remote sensing data (Anderson 1976).

The large proportion of vegetation patches are concentrated in the northern part of the city whilst small, scattered vegetation patches are concentrated in the western, eastern, and southern part of the city. In 1994, the amount of vegetation cover was approximately 27,190.8 (ha) and non-vegetation was 70,871.5 (ha). The proportion of vegetation in city declined to 26,575.5 (ha) in 2001 whilst non-vegetation was approximately 71,486.8 (ha). In 2010, the total area of

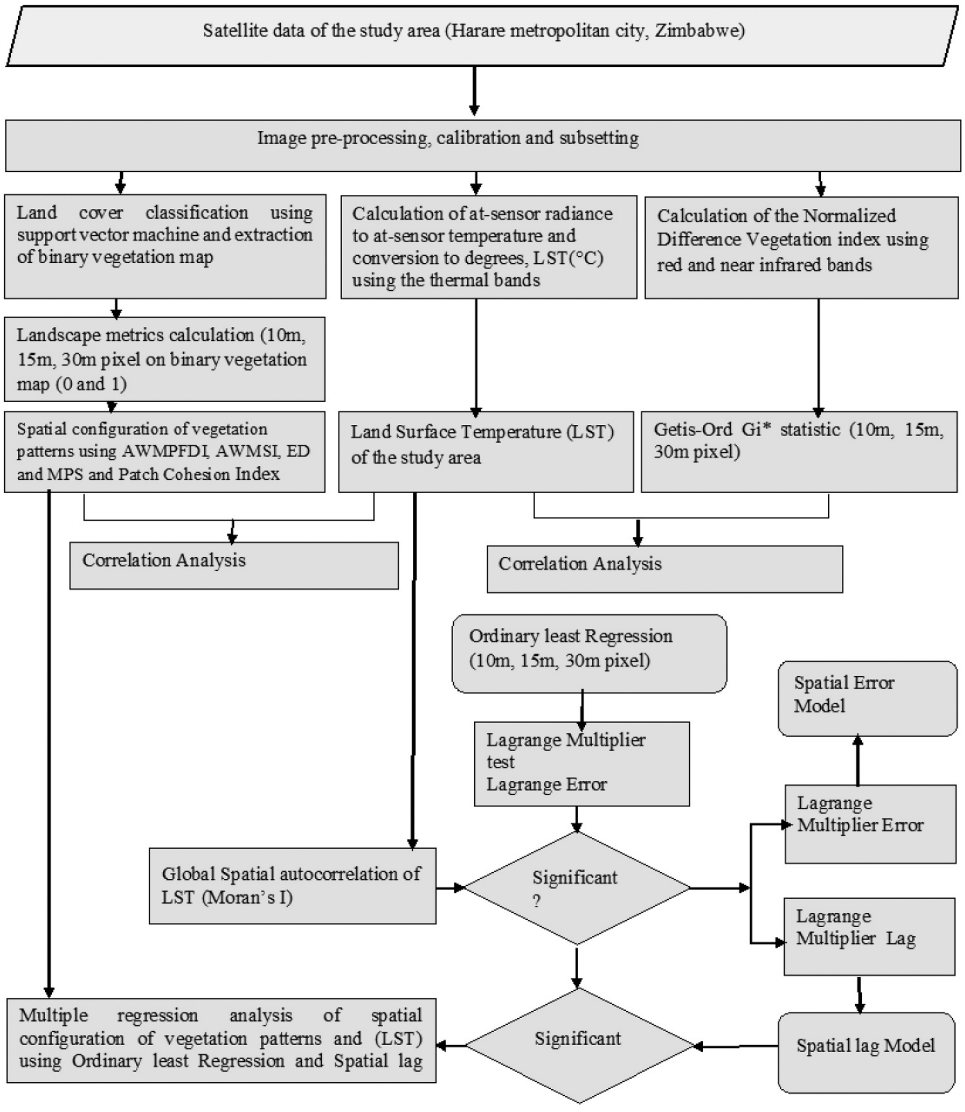

Figure 2. Flowchart of the research methodology and the steps presented in this study.

vegetation comprised 28,432.7 hectares (ha), and non-vegetation was 69,625.7 ha. In 2013, the total area of vegetation was approximately 25,377.2 ha and non-vegetation was around 72,687.24 ha. The total area of vegetation was 19,582.6 ha and non-vegetation was 78,480.9 ha on Landsat 8 acquired on October 23, 2017. On the other, the total area of vegetation was 25,958.6 ha and non-vegetation was 72,126.2 ha on Sentinel 2 acquired on October 24, 2017.

3.2 Spatial variability pattern of LST(°C)

(Table 3) shows the descriptive statistics of LST(°C) derived from Aster and Landsat data in 2010, 2013 and 2017. In 2010, the LST(°C) derived from ASTER data ranged from 18.89 to 45.50°C (Table 3). On the other hand, LST(°C) derived from Landsat data of 2013 ranged from 22.93 to 51.05°C. In 2017, it ranged from 23.81to 48.5°C. The mean LST(°C) value was 29.85°C in 1994, 31.80°C in 2001, 35.93°C in 2010, increased to 36.71°C in 2013 and 38.26°C in 2017 indicating the increasing warming trend in the study area. In 2010, 2013, and 2017, the significantly low values of LST(°C) dominated the northern side of the city suggesting the presence of dense vegetation and a cooler region

Table 3. Descriptive statistics of LST(°C).

Acquisition date	aMin (°C)	aMax (°C)	Mean (°C)	aSD
08/10/1994 (Landsat data)	14.71	41.45	29.85	3.27
19/10/2001 (Landsat data)	17.95	45.59	31.80	2.96
03/09/2010 (ASTER)	18.89	45.50	35.93	2.96
28/10/2013 (Landsat data)	22.93	51.05	36.71	3.58
23/10/2017 (Landsat data)	23.81	48.5	38.26	2.89

aMin-Minimum, *Max (Maximum), SD* (Standard Deviation).

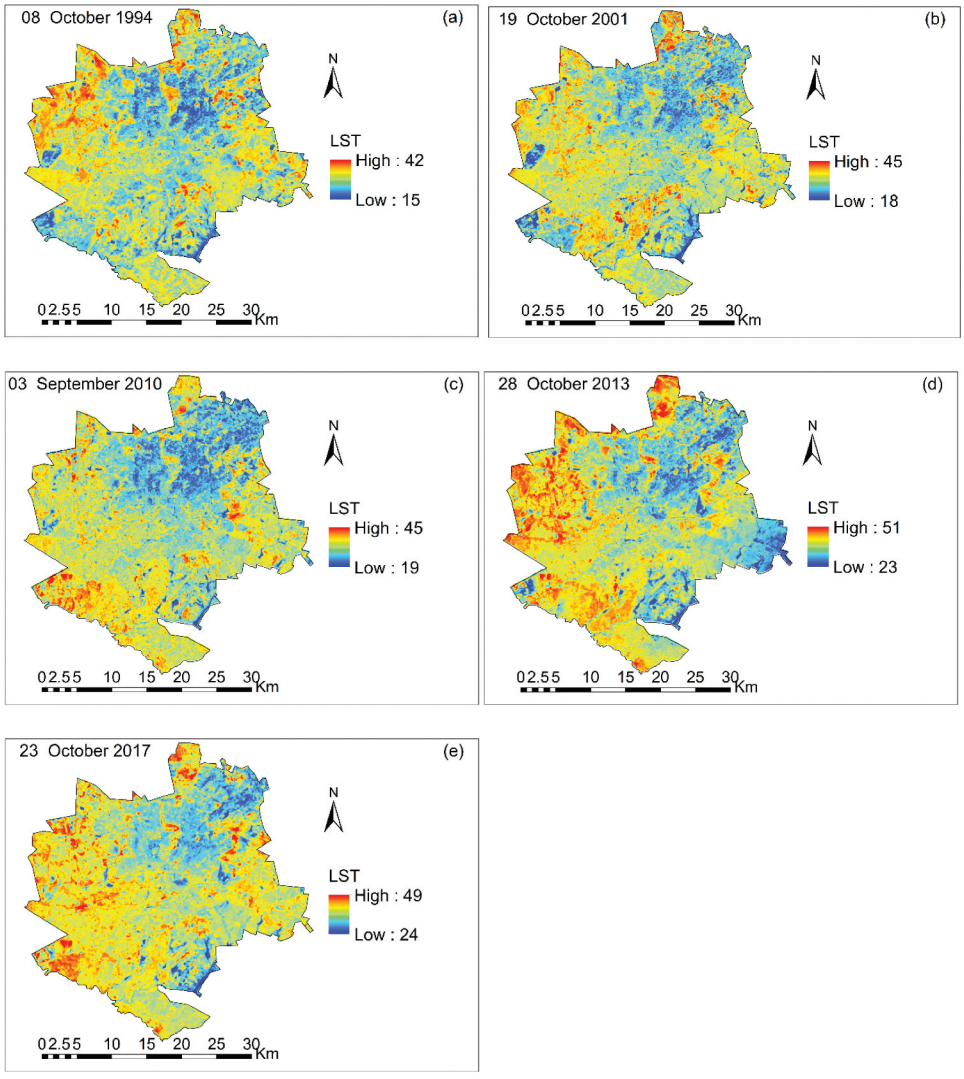

Figure 3. The spatial distribution of LST(°C) derived from a) Landsat 5 data acquired on 8 October 1994 (b) 19 October 2001 and (c) Aster data acquired on 9 September 2010 (d) 28 October 2013 and (e) 23 October 2017. Low values of LST(°C) are heavily concentrated in the northern side of the city and significantly high values of LST(°C) in the sparsely vegetated western, southern and eastern side of the city.

(Figure 3). On the other hand, significantly high values of LST(°C) dominate sparsely vegetated western, southern and eastern side of the city indicating a warmer region. The western, southern, and eastern side of the city is a densely built-up area with heavy concentration of industries and residential areas indicating the presence of impervious surfaces in raising higher land surface temperature.

3.3. *Effect of the spatial clustering and dispersion of vegetation on LST(°C)*

The Pearson correlation coefficients indicated the relatively moderate to strong negative linear relationship between LST(°C) and Getis-Ord Gi*.The relationships between the Getis-Ord Gi* and LST(°C) was ($r = -0.55$, $p < 0.05$) on Landsat data of 1994, ($r = -0.71$, $p < 0.05$) on Landsat data of 2001, ($r = -0.67$, $p < 0.05$) on Aster data of 2010, ($r = -0.60$, $p < 0.05$) on Landsat data of 2013, ($r = -0.60$, $p < 0.05$) on Sentinel 2 data of 2017 and ($r = -0.64$, $p < 0.05$) on Landsat data of 2017. This suggest that the spatial clustering of vegetation has strong impact in decreasing LST(°C) and correlate strongly with cooler surface temperatures. The spatial clustering of vegetation indicated by Getis Ord Gi* ranged from being dispersed (negative values), random (zero), and to highly clustered (positive values) as indicated in (Figure 4). The statistically significant high attribute values of Getis Ord

Gi* were heavily concentrated in the northern part of Harare, indicating that LST(°C) was low in areas with relatively high and positive clustering of vegetation (Figure 4). Conversely, LST(°C) was high in areas with low, negative clustering and dispersed vegetation patches in the western, southern, and eastern parts of the city (Figure 4). Therefore, higher LST(°C) closely correlate under dispersed and isolated vegetation patches, whereas lower LST(°C) correlate under high clustered vegetation patterns.

3.4 The relationship between spatial configuration of vegetation and LST(°C)

(Table 4) indicate that the landscape metrics of urban vegetation patterns had consistently negative relationships with LST(°C) ($p < 0.05$), but the magnitude of the correlation varied by spatial resolution at 10 m (Sentinel 2), 15 m (ASTER) and 30 m (Landsat 8). The Landsat acquired on on October 8, 1994 (b) October 19, 2001 were not considered for this analysis. The AWMPFDI, AWMSI, Edge Density and Mean Patch Size of landscape metrics were less correlated with LST(°C) at 30 m of Landsat 8 imagery data acquired on October 28, 2013 and October 23, 2017 than at 10 m (Sentinel 2) and 15 m (ASTER) spatial resolution. This suggests that the negative correlations between LST(°C) and landscape metrics of AWMPFDI, AWMSI, Edge Density, and Mean Patch size are stronger at finer spatial resolution.

MPS – Mean Patch Size, AWMPFDI – Area Weighted Mean Patch Fractal Dimension Index, AWMSI – Area

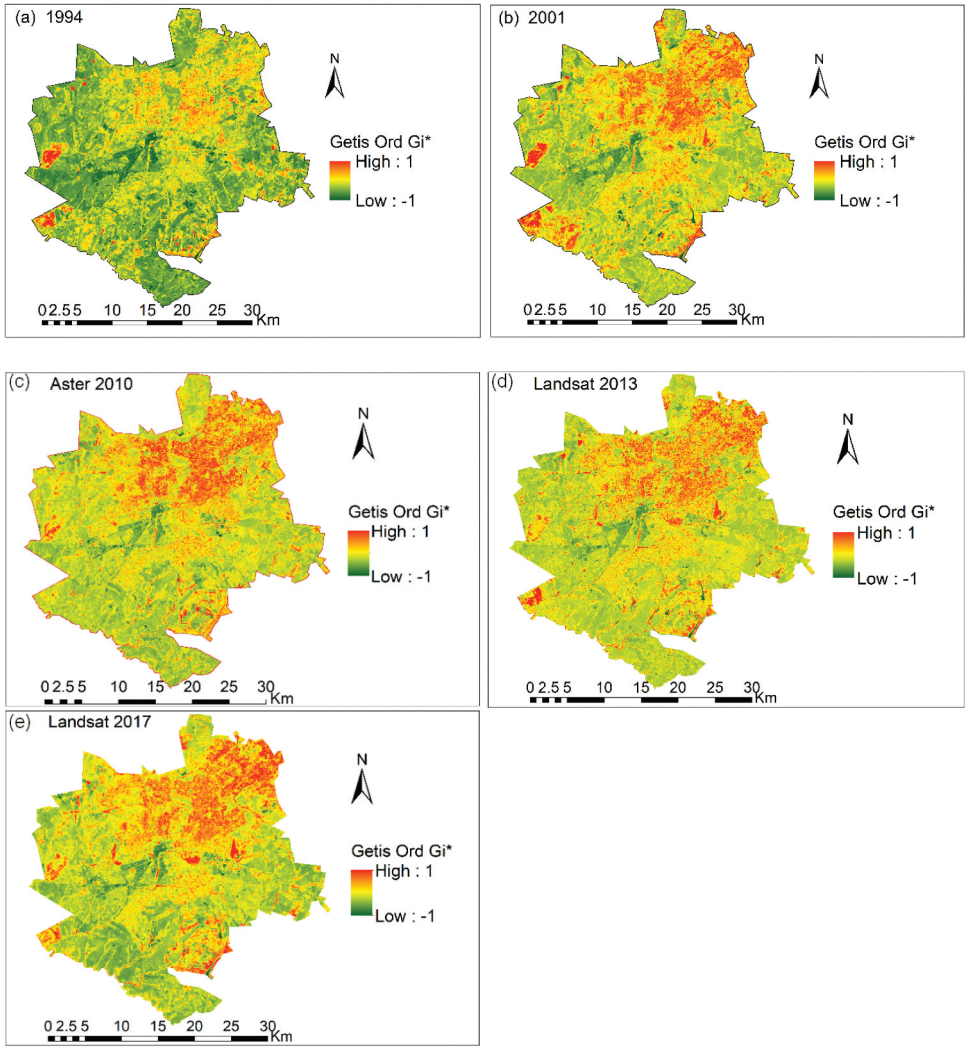

Figure 4. The spatial distribution of Getis-Ord Gi*) derived from a) Landsat 5 data acquired on 8 October 1994 (b) 19 October 2001 and (c) Aster data acquired on 9 September 2010 (d) 28 October 2013 and (e) 23 October 2017. High positive values of Getis-Ord Gi*represent highly clustered pattern and low and negative values represent highly dispersed patterns of vegetation.

Table 4. Pearson's correlation coefficients (r-values) showing the degree of associations between LST(°C) and landscape metrics.

	COHESION	MPS	ED	AWMSI	AWMPFDI
09/09/2010 ASTER (15 m)	−0.65	−0.26	−0.32	−0.37	−0.32
28/10/2013 (Landsat data) (30 m)	−0.68	−0.16	−0.21	−0.07	−0.09
23/10/2017 (Landsat data) (30 m)	−0.69	−0.15	−0.24	−0.08	−0.11
24/010/2017 (Sentinel 2) (10 m)	−0.61	−0.40	−0.37	−0.49	−0.34

Weighted Mean Shape Index, ED – Edge Density, COHESION -Patch Cohesion index.

Although all the landscape metrics had a significant negative correlation with LST(°C), however, Patch Cohesion index (COHESION) had the most consistently strong correlation with LST(°C) across all three spatial resolutions (10 m, 15 m, and 30 m) ($p < 0.05$). (Table 4) show that the Patch Cohesion index had relatively higher and stronger correlation at 30 m spatial resolution ($r = -0.69$, $p < 0.05$) in 2017 data and ($r = -0.68$, $p < 0.05$) in 2013 for Landsat 8 than at 10 m ($r = -0.61$, $p < 0.05$) for Sentinel 2 data acquired in 2017 and 15 m ($r = -0.65$, $p < 0.05$) for ASTER data of 2010 as indicated in (Table 4). This suggests that the relationship between LST(°C) and Patch Cohesion index increase with the subsequent decrease of spatial resolution. In addition, the results of the Patch Cohesion index may indicate that highly connected and less isolated vegetation patterns do have a strong cooling effect and have a strong impact in decreasing LST(°C). Higher vegetation connectivity (i.e., less isolation of vegetation patches) are associated with a greater proportion of high, contiguous vegetation patterns, reflecting shorter distances between the vegetation patches and may contribute to lower and minimum LST(°C) values (e.g. 18°C, 22 and 23°C) as indicated in (Figure 5). These are illustrated with higher vegetation connectivity ranges (<50%-70%).

On the other hand, lower vegetation connectivity (higher degree of isolation of vegetation patches) contributes to higher and maximum LST(°C) values (e.g., 45°C, 48°C, and 51°C) as illustrated in (Figure 5). Areas with less connected vegetation are found in the western, southern and eastern side of the city. These are illustrated with lower vegetation connectivity ranges (<0–30%). Less connected vegetation (<0–30%) represent the highly fragmented nature of vegetation patches that are smaller, isolated, and scattered across the landscape.

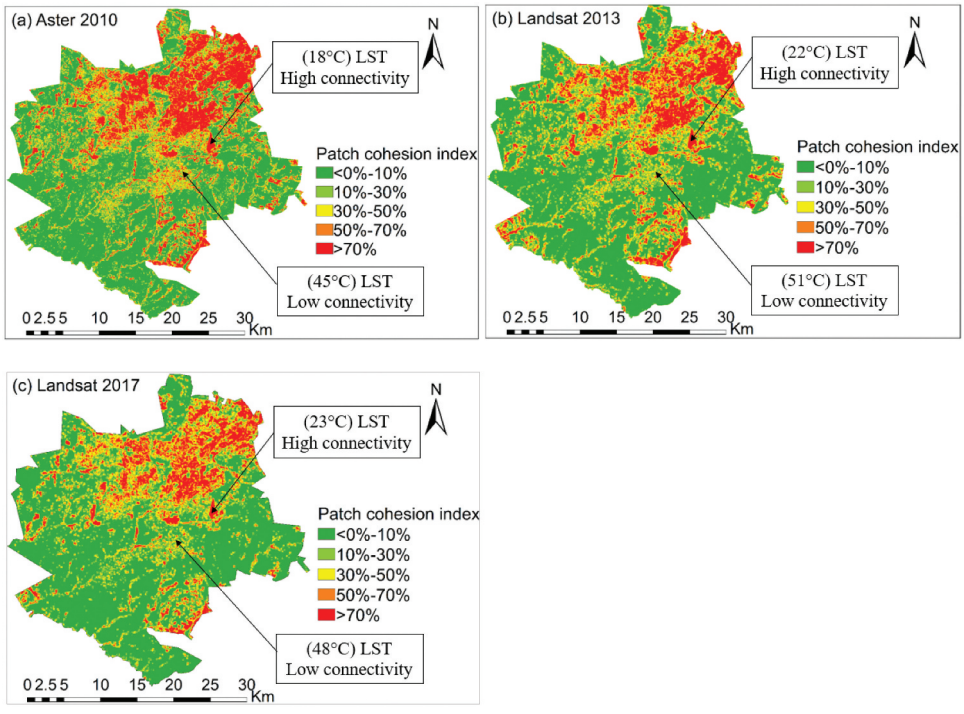

Figure 5. Patch cohesion index derived from (a) Aster data of 2010 (b) Landsat data of 2013 and (c) Landsat data of 2017 illustrating that high vegetation connectivity correspond to lower LST(°C) and vice versa.

3.5 Spatial autocorrelation of LST(°C)

There was significant spatial autocorrelation of LST(°C) which meant that similar LST(°C) were clustered together in the study area. (Table 5) indicate that the Moran's I value for LST(°C) was 0.21 for Sentinel 2 of 2017, 0.18 for Aster data of 2010, and 0.27 ($p < 0.001$) for Landsat 8 of 2017 data which meant that there was less than a 0.1% chance that the observed spatial clustering pattern in the study was due to random chance. Due to the significant spatial autocorrelation of LST(°C) in the study area, it meant that the results of the Ordinary Least Squares model regression model would have been misleading without the adoption of a spatial regression model since the conventional OLS regression model violated the independent observations and uncorrelated error assumptions.

3.6 Comparisons of OLS and SLM regression models

(Table 5) shows the results of Model 1 (Ordinary Least Squares model) and Model 2 (Spatial lag regression model) that examined the relationships between mean LST(°C) and spatial configurations of vegetation based on landscape metrics as independent variables at different spatial resolutions. The landscape metrics included ED, MPS, AWMSI, AWMPFD, and Patch Cohesion Index. The three different spatial resolutions were based on 10 m spatial resolution (Sentinel 2) acquired on October 24, 2017, 15 m spatial resolution (ASTER) acquired on September 9, 2010, and 30 m spatial resolution (Landsat 8) acquired on October 23, 2017. The Landsat acquired on October 28, 2013 was not considered. The Model 1(OLS) explained about 11% ($R^2 = 0.1058$) for Sentinel 2 (10 m), 13% ($R^2 = 0.1304$) for Aster data (15 m) and 53% ($R^2 = 0.5285$) for Landsat 8 data (30 m) of the variance in the relationship between mean LST(°C) and landscape metrics.

On the other hand, Model 2 (SLM) explained 51% ($R^2 = 0.5076$) for Sentinel 2 (10 m), 52% ($R^2 = 0.5153$) for Aster data (15 m) and 64% ($R^2 = 0.6353$) for Landsat 8 data (30 m) of the variance in the relationship between mean LST(°C) and spatial configuration of vegetation. This indicates that more than 50% of the variations in mean LST(°C) can be explained by the selected landscape metrics in SLM model. In both models, R2 values become higher with the decrease of the spatial resolution.

Besides higher R2 values, the results obtained by SLM (Model 2) are characterized by higher log likelihood in SLM model than those in OLS model. Both AIC and Schwarz criteria were smaller in SLM model than those in OLS model indicating that the that spatial regression was superior to the traditional regression method of OLS. The comparison of these two models suggests that the SLM model performs better than OLS model for investigating the relationships between mean LST(°C) and spatial configurations of vegetation.

4.0 Discussion

This study examined the effect of landscape pattern and spatial configuration of vegetation patches on land surface temperature in Harare metropolitan city in significantly enhancing or mitigating the urban warming. The study showed that the effect of spatial configuration of vegetation on LST(°C) significantly vary with a particular landscape metrics used. The results of Pearson's correlation coefficient of LST(°C) with landscape metrics suggest that highly connected, irregularly shaped vegetation patterns, patch size and green space edge (conditions significantly reduce LST(°C). This is consistent with previous studies that show that the landscape metrics of vegetation were significantly correlated with LST(°C) (Kong et al. 2014a, Maimaitiyiming et al. 2014; Li et al. 2012; Zhang et al. 2009; Zhou, Huang, and Cadenasso 2011).

Table 5. Results of Ordinary Least Squares (OLS) and Spatial Lag regression Model (SLM) analysis.

	Models					
	Model 1: OLS			Model 2: SLM		
Parameter	Sentinel 2 (10 m)	ASTER (15 m)	Landsat 8 (30 m)	Sentinel 2 (10 m)	ASTER (15 m)	Landsat 8 (30 m)
R-squared (R^2)	0.11	0.13	0.53	0.51	0.52	0.64
LL	−110,805	−58,143.7	−26,092.2	−98,932.8	−51,344.8	−24,594.7
AIC	221,621	116,299	52,196.4	197,880	102,704	49,203.4
SC	221,674	116,348	52,241.2	197,941	102,761	49,255.7
Moran's I	0.21	0.18	0.27			

LL-log likelihood; AIC-Akaike information criterion; and SC-Schwarz criterion

This is largely because different landscape patterns and configurations such as the shape, size, connectivity, and edge density can influence the thermal exchange between vegetation and its surroundings, further inducing different warmings and cooling effects.

Li et al. (2012) found a negative relationship between LST(°C) and the shape complexity and mean patch size of the patches of green space in Beijing, China. Green spaces with more complex shapes were shown to deliver higher cooling effects in several studies (Asgarian, Amiri, and Sakieh 2015; Bao et al. 2016, Kong et al. 2014a; Li et al. 2012; Zhang et al. 2009; Zhou, Huang, and Cadenasso 2011). In our study, the negative correlation between the LST(°C) and shape complexity were relatively higher on AWMSI than AWMPFD. This is not surprising as in calculating the average patch shape complexity, AWMSI weights larger patches more heavily than smaller patches. The negative correlations between edge density of vegetation patches with LST(°C) were observed in the Mediterranean cities of Europe (Nastran, Kobal, and Eler 2019), Aksu city in China (Maimaitiyiming et al. 2014) and in Baltimore in USA (Zhou, Huang, and Cadenasso 2011). Zhou, Huang, and Cadenasso (2011) noted that LST(°C) decreased through the increase in the amount of green space edge (edge density), which enhances the energy flow and thermal exchange between the urban green space and its surrounding areas and provide more shade for surrounding surfaces.

The green vegetation patches are larger, more complex, and more contiguous in the northern part of Harare whereas in the western, southern, and eastern parts portion of the city, they are mostly fragmented and dispersed. Previous investigation by Mushore et al. (2017) reported higher LST(°C) in the sparsely vegetated western, southern and eastern side of the city. Small green spaces usually have a high thermal load and are unlikely to produce significant cooling effects (Bao et al. 2016). Conversely, the densely vegetated northern part of Harare had consistently lower LST(°C). Larger, contiguous vegetation patches have been found in previous studies to produce stronger cooling effects than that of several smaller and isolated vegetation patches (Maimaitiyiming et al. 2014; Li et al. 2012; Zhang et al. 2009). Large and dense vegetation patches are more heat tolerant producing cooling effects during daytime that greatly offset the warming effects caused by the small, isolated vegetation and the built-up and impervious surfaces. Dugord et al. (2014) also reported that larger forest share and extensive, aggregated forest patches significantly reduced LST(°C) in Berlin.

The strength of the Getis-Ord Gi* is its ability to provide continuous representation of the true heterogeneity of the landscape. Based on a Getis-Ord Gi*,, our findings are consistent with previous studies that indicate that less fragmented patterns of urban vegetation lower LST(°C) more effectively (Fan, Myint, and Zheng 2015; Peng et al. 2016) than more fragmented (dispersed) patterns of urban vegetation that raise LST(°C) as indicated in (Li et al. 2012; Zhang et al. 2009). Clustered patches of vegetation may increase latent heat fluxes through evaporation, thereby reducing the sensible heat emitted from the surface. Furthermore, clustered vegetation patches shade the surface by absorbing incipient solar radiation, which substantially lowers the land surface temperature.

4.1 Effect of spatial resolution on LST(°C) and landscape metrics relationship

The effect of landscape metrics of vegetation on LST(°C) were affected by the spatial resolution of the satellite imagery data, which confirms the previous findings of other studies (Li, Zhou, and Ouyang 2013). With the exception of Patch Cohesion index, the correlation coefficients of LST(°C) with landscape metrics of AWMPFDI, AWMSI, Edge Density, and Mean Patch size declined significantly with the decrease of spatial resolution becoming stronger at finer spatial resolution of 10 m (Sentinel 2) and 15 m (ASTER) than at 30 m (Landsat 8). This is probably due to the fact that finer rather than low satellite imagery data effectively extract the large distribution number of small, isolated vegetation patches in urban areas. This also explains, a non-significant and low correlation coefficient between LST(°C) and landscape metrics of AWMPFDI, AWMSI, ED, Edge Density, and Mean Patch size at 30 m Landsat 8 imagery data.

On the other hand, several reasons can be highlighted in explaining the higher negative correlation between LST(°C) and Patch Cohesion index at 30 m ($r = -0.69$) than at 15 m ($r = -0.65$) and 10 m ($r = -0.61$) resolutions. One of the reasons is that, Patch Cohesion index is sensitive to the aggregation of the focal class or patch type (McGarigal 2002). It increases as the

patch type becomes more clumped or aggregated in its distribution, consequently creating a physically connected patch (Gustafson 1998). Hence, Patch Cohesion index tends to be biased toward larger patches than smaller patches. In low and medium resolution image data such as the 30 m resolution (Landsat 8), small patch sizes of vegetation easily identified from the fine resolution imagery may be mapped as one single large vegetation patch. Patch Cohesion index has been previously found to report lower fragmentation at coarser spatial resolutions (Saura 2004).

4.2 The advantages of SLM model over OLS model

The selection of a suitable spatial regression method and local statistical model is essential in analyzing the relationship between the UHI effect and landscape factors of vegetation pattern. This study, by comparing both the OLS regression model and SLM spatial regression model, found that, all the parameters such as R^2, log-likelihood, Akaike information criterion (AIC) and Schwarz criteria in OLS regression model were not as good as those in the SLM. SLM model performed better than OLS model in examining the relationships between mean LST(°C) and spatial configurations of vegetation. Furthermore, SLM model had stronger explanatory power and lower spatial autocorrelations of residuals compared with conventional OLS model.

Significant positive spatial autocorrelations in residuals based on Moran's I values were detected in the OLS model. Hence, the assumption of randomly distributed and residual independence is violated when applying OLS in analyzing the relationship between the urban surface temperature and driving landscape factors of vegetation pattern. OLS regression cannot take into account the spatial autocorrelation of the dependent variables, thus making the model misleading which may limit the predictive utility of understanding the mitigation of the UHI effect and specific local planning of cities and urban areas.

Traditional regression methods, such as the OLS regression model are "global" models that assumed to apply global parameters over an entire geographical area which best describes the overall data relationships in a study area which calls for the need for a local estimations and predictions to the specific local region or geographical area. As opposed to OLS model, which may mask out local spatial variations, SLM is a localized spatial regression method that examines spatially non-stationary phenomena of urban surface temperature by generating local slope coefficients of driving landscape factors of vegetation pattern.

LST is spatially autocorrelated because of land surface heat fluxes (Song et al. 2014). Specifically, SLM has the potential to solve the problem related to spatial dependence when the dependent variable is influenced by nearby locations in the study area. Ordinary least squares analysis does not take spatial autocorrelation into account. These findings confirm the observation of previous studies that emphasize the use of spatial regression methods (Li et al. 2012) which are needed when examining the relationships between mean LST(°C) and spatial configurations of vegetation. This is because spatial regression methods provide more robust evidence on the relationships between spatial configurations of vegetation and LST(°C) in minimizing spatial autocorrelation in spatial datasets.

5.0 Conclusions and recommendations

Understanding the landscape pattern and configuration of green spaces could help urban planners and conservationists in urban and green infrastructure planning for climate adaptation and mitigate UHI effect in rapid growing cities and sprawling metropolitan regions. In general, dispersed or fragmented vegetation is less effective in mitigating the urban warming effect than clustered or clumped vegetation. Hence, it is recommended that urban planners and policy makers should optimize the spatial arrangements and configurations of urban landscapes by aggregating or clustering vegetation. This will promote the effective urban planning practices by improving landscape design and land use management. Due to continuing green spaces fragmentation in urban areas, urban design and planning should account for green spaces that are relatively fragmented and scattered to maximize the cooling effects.

However, the landscape metrics of urban green spaces and their relationships with LST(°C) are sensitive to spatial resolution. Satellite imagery data with higher spatial resolution could more accurately quantify the spatial configuration of urban vegetation. The effects of finer spatial resolution generally had better correlation coefficients with land surface temperature providing important indications of the spatial resolutions at which maximum warming and cooling effect

is achieved. In developing more insights into the relationship between spatial configuration of urban vegetation and LST(°C), it is suggested that spatial regression methods be utilized in future studies dealing with spatial data where the fundamental assumption of spatial dependency is more often than not violated. In general, this study demonstrated that the landscape metrics can convey meaningful information on the spatial configuration of vegetation and its effects on different levels of cooling in a landscape.

Acknowledgments

This work was supported by the This work is based on the research supported by the Department of Science and Technology (DST)/National Research Foundation (NRF) of South Africa (Grant Numbers: 84,157) and the authors would like to thank and acknowledge the NRF Chair in Land Use Planning and Management for this financial assistance.

Article Highlights

- The effect of spatial configuration of vegetation on the land surface temperature was quantified.
- Higher, clustered, and less fragmented vegetation is associated with a lower urban heat island in northern Harare.
- Smaller, dispersed, and scattered patches of vegetation increase the urban heat island in western, eastern, and southern Harare.
- Patch cohesion index had the most consistently strong correlation with land surface temperature.
- Spatial regressions were used to account for spatial autocorrelation of the dependent variable of LST(°C).

Disclosure statement

There are no conflicts of interest. We declare that we have no affiliations with or involvement in any organization, people, or entity with any financial interest, or non-financial interest in the subject matter or materials discussed that could be construed as influencing the position presented in the manuscript.

Funding

This research work was financially supported by the Department of Science and Technology (DST)/National Research Foundation (NRF) of South Africa Chair in Land Use Planning and Management (Grant Numbers: 84157).

References

Adams, M. P., and P. L. Smith. 2014. "A Systematic Approach to Model the Influence of the Type and Density of Vegetation Cover on Urban Heat Using Remote Sensing." *Landscape and Urban Planning* 132: 47–54. doi:10.1016/j.landurbplan.2014.08.008.

Adeyeri, O. E., A. A. Akinsanola, and K. A. Ishola. 2017. "Investigating Surface Urban Heat Island Characteristics over Abuja, Nigeria: Relationship between Land Surface Temperature and Multiple Vegetation Indices." *Remote Sensing Applications: Society and Environment* 7: 57–68. doi:10.1016/j.rsase.2017.06.005.

Akbari, H., C. Cartalis, D. Kolokotsa, A. Muscio, A. L. Pisello, F. Rossi, M. Santamouris, A. Synnefa, N. H. Wong, and M. Zinzi. 2016. "Local Climate Change and Urban Heat Island Mitigation Techniques–the State of the Art." *Journal of Civil Engineering and Management* 22 (1): 1–16. doi:10.3846/13923730.2015.1111934.

Anderson, J. R. 1976. "A Land Use and Land Cover Classification System for Use with Remote Sensor Data (Vol. 964)." US Government Printing Office

Anselin, L. 1995. "Local Indicators of Spatial association—LISA." *Geographical Analysis* 27 (2): 93–115. doi:10.1111/j.1538-4632.1995.tb00338.x.

Anselin, L., I. Syabri, and Y. Kho. 2006. "GeoDa: An Introduction to Spatial Data Analysis." *Geographical Analysis* 38 (1): 5–22. doi:10.1111/j.0016-7363.2005.00671.x.

Anselin, L. 2003. "An Introduction to Spatial Autocorrelation Analysis with GeoDa." Spatial Analysis Laboratory, University of Illinois, Champagne-Urbana, Illinois.

Aram, F., E. H. García, E. Solgi, and S. Mansournia. 2019. "Urban Green Space Cooling Effect in Cities." *Heliyon* 5 (4): e01339. doi:10.1016/j.heliyon.2019.e01339.

Arnold, C. L., Jr, and C. J. Gibbons. 1996. "Impervious Surface Coverage: The Emergence of a Key Environmental Indicator." *Journal of the American Planning Association* 62 (2): 243–258. doi:10.1080/01944369608975688.

Asgarian, A., B. J. Amiri, and Y. Sakieh. 2015. "Assessing the Effect of Green Cover Spatial Patterns on Urban Land Surface Temperature Using Landscape Metrics Approach." *Urban Ecosystems* 18 (1): 209–222. doi:10.1007/s11252-014-0387-7.

Bao, T., X. Li, J. Zhang, Y. Zhang, and S. Tian. 2016. "Assessing the Distribution of Urban Green Spaces and Its Anisotropic Cooling Distance on Urban Heat Island Pattern in Baotou, China." *ISPRS International Journal of Geo-Information* 5 (2): 12. doi:10.3390/ijgi5020012.

Berger, C., J. Rosentreter, M. Voltersen, C. Baumgart, C. Schmullius, and S. Hese. 2017. "Spatio-temporal Analysis of the Relationship between 2D/3D Urban Site Characteristics and Land Surface Temperature." *Remote Sensing of Environment* 193: 225–243. doi:10.1016/j.rse.2017.02.020.

Buyantuyev, A., and J. Wu. 2010. "Urban Heat Islands and Landscape Heterogeneity: Linking Spatiotemporal Variations in Surface Temperatures to Land-cover and

Socioeconomic Patterns." *Landscape Ecology* 25 (1): 17–33. doi:10.1007/s10980-009-9402-4.

Carlson, T. N., and D. A. Ripley. 1997. "On the Relation between NDVI, Fractional Vegetation Cover, and Leaf Area Index." *Remote Sensing of Environment* 62 (3): 241–252. doi:10.1016/S0034-4257(97)00104-1.

Chander, G., and B. Markham. 2003. "Revised Landsat-5 TM Radiometric Calibration Procedures and Post Calibration Dynamic Ranges." *IEEE Transactions on Geoscience and Remote Sensing* 41 (11): 2674–2677. doi:10.1109/TGRS.2003.818464.

Chander, G., B. L. Markham, and D. L. Helder. 2009. "Summary of Current Radiometric Calibration Coefficients for Landsat MSS, TM, ETM+, and EO-1 ALI Sensors." *Remote Sensing of Environment* 113 (5): 893–903. doi:10.1016/j.rse.2009.01.007.

Chen, A., X. A. Yao, R. Sun, and L. Chen. 2014. "Effect of Urban Green Patterns on Surface Urban Cool Islands and Its Seasonal Variations." *Urban Forestry & Urban Greening* 13 (4): 646–654. doi:10.1016/j.ufug.2014.07.006.

Chen, A., X. Zhao, L. Yao, and L. Chen. 2016. "Application of a New Integrated Landscape Index to Predict Potential Urban Heat Islands." *Ecological Indicators* 69: 828–835. doi:10.1016/j.ecolind.2016.05.045.

Chen, X. L., H. M. Zhao, P. X. Li, and Z. Y. Yin. 2006. "Remote Sensing Image-based Analysis of the Relationship between Urban Heat Island and Land Use/cover Changes." *Remote Sensing of Environment* 104 (2): 133–146. doi:10.1016/j.rse.2005.11.016.

Chen, Y. C., H. W. Chiu, Y. F. Su, Y. C. Wu, and K. S. Cheng. 2017. "Does Urbanization Increase Diurnal Land Surface Temperature Variation? Evidence and Implications." *Landscape and Urban Planning* 157: 247–258. doi:10.1016/j.landurbplan.2016.06.014.

Chopin, P., and J. M. Blazy. 2013. "Assessment of Regional Variability in Crop Yields with Spatial Autocorrelation: Banana Farms and Policy Implications in Martinique." *Agriculture, Ecosystems & Environment* 181: 12–21. doi:10.1016/j.agee.2013.09.001.

Cliff, A. D., and J. K. Ord. 1981. *Spatial Processes: Models & Applications*. London: Taylor & Francis.

Congalton, R. G., and K. Green. 1999. *Assessing the Accuracy of Remotely Sensed Data: Principles and Practices*, 43–64. Boca Rotan: Florida'Lewis Publishers.

Connors, J. P., C. S. Galletti, and W. T. Chow. 2013. "Landscape Configuration and Urban Heat Island Effects: Assessing the Relationship between Landscape Characteristics and Land Surface Temperature in Phoenix, Arizona." *Landscape Ecology* 28 (2): 271–283. doi:10.1007/s10980-012-9833-1.

Craglia, M., R. Haining, and P. Wiles. 2000. "A Comparative Evaluation of Approaches to Urban Crime Pattern Analysis." *Urban Studies* 37 (4): 711–729. doi:10.1080/00420980050003982.

Dobbs, C., C. R. Nitschke, and D. Kendal. 2014. "Global Drivers and Tradeoffs of Three Urban Vegetation Ecosystem Services." *PLoS One* 9 (11): e113000. doi:10.1371/journal.pone.0113000.

Dugord, P. A., S. Lauf, C. Schuster, and B. Kleinschmit. 2014. "Land Use Patterns, Temperature Distribution, and Potential Heat Stress Risk–the Case Study Berlin, Germany." *Computers, Environment and Urban Systems* 48: 86–98. doi:10.1016/j.compenvurbsys.2014.07.005

Estoque, R. C., Y. Murayama, and S. W. Myint. 2017. "Effects of Landscape Composition and Pattern on Land Surface Temperature: An Urban Heat Island Study in the Megacities of Southeast Asia." *Science of the Total Environment* 577: 349–359. doi:10.1016/j.scitotenv.2016.10.195.

Fan, C., and S. Myint. 2014. "A Comparison of Spatial Autocorrelation Indices and Landscape Metrics in Measuring Urban Landscape Fragmentation." *Landscape and Urban Planning* 121: 117–128. doi:10.1016/j.landurbplan.2013.10.002.

Fan, C., S. W. Myint, and B. Zheng. 2015. "Measuring the Spatial Arrangement of Urban Vegetation and Its Impacts on Seasonal Surface Temperatures." *Progress in Physical Geography* 39 (2): 199–219. doi:10.1177/0309133314567583.

Farhadi, H., M. Faizi, and H. Sanaieian. 2019. "Mitigating the Urban Heat Island in a Residential Area in Tehran: Investigating the Role of Vegetation, Materials, and Orientation of Buildings." *Sustainable Cities and Society* 46: 101448. doi:10.1016/j.scs.2019.101448.

Feyisa, G. L., K. Dons, and H. Meilby. 2014. "Efficiency of Parks in Mitigating Urban Heat Island Effect: An Example from Addis Ababa." *Landscape and Urban Planning* 123: 87–95. doi:10.1016/j.landurbplan.2013.12.008.

Forman, R. T. 1995. "Some General Principles of Landscape and Regional Ecology." *Landscape Ecology* 10 (3): 133–142. doi:10.1007/BF00133027.

Gabriel, K. M., and W. R. Endlicher. 2011. "Urban and Rural Mortality Rates during Heat Waves in Berlin and Brandenburg, Germany." *Environmental Pollution* 159 (8–9): 2044–2050. doi:10.1016/j.envpol.2011.01.016.

Getis, A., and J. K. Ord. 1992. "The Analysis of Spatial Association by Use of Distance Statistics." *Geographical Analysis* 24: 189–206. doi:10.1111/j.1538-4632.1992.tb00261.x.

Gill, S. E., J. F. Handley, A. R. Ennos, and S. Pauleit. 2007. "Adapting Cities for Climate Change: The Role of the Green Infrastructure." *Built Environment* 33 (1): 115–133. doi:10.2148/benv.33.1.115.

Guhathakurta, S., and P. Gober. 2007. "The Impact of the Phoenix Urban Heat Island on Residential Water Use." *Journal of the American Planning Association* 73 (3): 317–329. doi:10.1080/01944360708977980.

Gustafson, E. J. 1998. "Quantifying Landscape Spatial Pattern: What Is the State of the Art?" *Ecosystems* 1 (2): 143–156. doi:10.1007/s100219900011.

Hamada, S., T. Tanaka, and T. Ohta. 2013. "Impacts of Land Use and Topography on the Cooling Effect of Green Areas on Surrounding Urban Areas." *Urban Forestry & Urban Greening* 12 (4): 426–434. doi:10.1016/j.ufug.2013.06.008

Huang, G., and M. L. Cadenasso. 2016. "People, Landscape, and Urban Heat Island: Dynamics among Neighborhood Social Conditions, Land Cover and Surface Temperatures."

Landscape Ecology 31 (10): 2507–2515. doi:10.1007/s10980-016-0437-z.

Kamusoko, C., J. Gamba, and H. Murakami. 2013. "Monitoring Urban Spatial Growth in Harare Metropolitan Province, Zimbabwe." *Advances in Remote Sensing* 2 (4): 322–331. doi:10.4236/ars.2013.24035.

Kong, F., H. Yin, P. James, L. R. Hutyra, and H. S. He. 2014a. "Effects of Spatial Pattern of Greenspace on Urban Cooling in a Large Metropolitan Area of Eastern China." *Landscape and Urban Planning* 128: 35–47. doi:10.1016/j.landurbplan.2014.04.018.

Kong, F., H. Yin, C. Wang, G. Cavan, and P. James. 2014b. "A Satellite Image-based Analysis of Factors Contributing to the Green-space Cool Island Intensity on A City Scale." *Urban Forestry & Urban Greening* 13 (4): 846–853. doi:10.1016/j.ufug.2014.09.009.

Lai, D., W. Liu, T. Gan, K. Liu, and Q. Chen. 2019. "A Review of Mitigating Strategies to Improve the Thermal Environment and Thermal Comfort in Urban Outdoor Spaces." *Science of the Total Environment* 661: 337–353. doi:10.1016/j.scitotenv.2019.01.062.

Lai, L. W., and W. L. Cheng. 2009. "Air Quality Influenced by Urban Heat Island Coupled with Synoptic Weather Patterns." *Science of the Total Environment* 407 (8): 2724–2733. doi:10.1016/j.scitotenv.2008.12.002.

Legendre, P., and M. J. Fortin. 1989. "Spatial Pattern and Ecological Analysis." *Vegetatio* 80 (2): 107–138. doi:10.1007/BF00048036.

Li, J., C. Song, L. Cao, F. Zhu, X. Meng, and J. Wu. 2011. "Impacts of Landscape Structure on Surface Urban Heat Islands: A Case Study of Shanghai, China." *Remote Sensing of Environment* 115 (12): 3249–3263. doi:10.1016/j.rse.2011.07.008.

Li, X., W. Li, A. Middel, S. L. Harlan, A. J. Brazel, and B. L. Turner Ii. 2016. "Remote Sensing of the Surface Urban Heat Island and Land Architecture in Phoenix, Arizona: Combined Effects of Land Composition and Configuration and Cadastral–demographic–economic Factors." *Remote Sensing of Environment* 174: 233–243. doi:10.1016/j.rse.2015.12.022.

Li, X., W. Zhou, and Z. Ouyang. 2013. "Relationship between Land Surface Temperature and Spatial Pattern of Greenspace: What are the Effects of Spatial Resolution?" *Landscape and Urban Planning* 114: 1–8. doi:10.1016/j.landurbplan.2013.02.005.

Li, X., W. Zhou, Z. Ouyang, W. Xu, and H. Zheng. 2012. "Spatial Pattern of Greenspace Affects Land Surface Temperature: Evidence from the Heavily Urbanized Beijing Metropolitan Area, China." *Landscape Ecology* 27 (6): 887–898. doi:10.1007/s10980-012-9731-6.

Li, X., Y. Zhou, G. R. Asrar, M. Imhoff, and X. Li. 2017. "The Surface Urban Heat Island Response to Urban Expansion: A Panel Analysis for the Conterminous United States." *Science of the Total Environment* 605: 426–435. doi:10.1016/j.scitotenv.2017.06.229.

Liu, D., Q. Zhao, S. Guo, P. Liu, L. Xiong, X. Yu, H. Zou, Y. Zeng, and Z. Wang. 2019. "Variability of Spatial Patterns of Autocorrelation and Heterogeneity Embedded in Precipitation." *Hydrology Research* 50 (1): 215–230. doi:10.2166/nh.2018.054.

Maimaitiyiming, M., A. Ghulam, T. Tiyip, F. Pla, P. Latorre-Carmona, Ü. Halik, M. Sawut, and M. Caetano. 2014. "Effects of Green Space Spatial Pattern on Land Surface Temperature: Implications for Sustainable Urban Planning and Climate Change Adaptation." *ISPRS Journal of Photogrammetry and Remote Sensing* 89: 59–66. doi:10.1016/j.isprsjprs.2013.12.010.

Masoudi, M., P. Y. Tan, and S. C. Liew. 2019. "Multi-city Comparison of the Relationships between Spatial Pattern and Cooling Effect of Urban Green Spaces in Four Major Asian Cities." *Ecological Indicators* 98: 200–213. doi:10.1016/j.ecolind.2018.09.058.

McGarigal, K. 2002. "FRAGSTATS: Spatial Pattern Analysis Program for Categorical Maps" *Computer software program produced by the authors at the University of Massachusetts*, Amherst. http://www.umass.edu/landeco/research/fragstats/fragstats.html.

McGarigal, K., and S. Cushman. 2005. "The Gradient Concept of Landscape Structure [Chapter 12]." J. A. Wiens and M. R. Moss edited by. *Issues and Perspectives in Landscape Ecology*. 112–119. Washington, DC: Cambridge University Press.

McGarigal, K., and B. J. Marks. 1995. ":FRAGSTATS: Spatial Pattern Analysis Program for Quantifying Landscape Structure." Gen. Tech. Rep. PNW-GTR-351. Portland, OR: US Department of Agriculture, Forest Service, Pacific Northwest Research Station. 122 p, 351.

McGarigal, K., S. Tagil, and S. A. Cushman. 2009. "Surface Metrics: An Alternative to Patch Metrics for the Quantification of Landscape Structure." *Landscape Ecology* 24 (3): 433–450. doi:10.1007/s10980-009-9327-y.

Moran, P. A. 1950. "Notes on Continuous Stochastic Phenomena." *Biometrika* 37 (1/2): 17–23. doi:10.1093/biomet/37.1-2.17.

Mushore, T. D., O. Mutanga, J. Odindi, and T. Dube. 2017. "Linking Major Shifts in Land Surface Temperatures to Long Term Land Use and Land Cover Changes: A Case of Harare, Zimbabwe." *Urban Climate* 20: 120–134. doi:10.1016/j.uclim.2017.04.005.

Myint, S. W. 2012. "Effects of the Spatial Pattern of Vegetation Cover on Urban Warming in a Desert City." In Yang and J. Li (Eds.), *Advances in Mapping from Aerospace Imagery: Techniques and Applications*, 261–278. Boca Raton, FL: CRC Press.

Myint, S. W., E. A. Wentz, A. J. Brazel, and D. A. Quattrochi. 2013. "The Impact of Distinct Anthropogenic and Vegetation Features on Urban Warming." *Landscape Ecology* 28 (5): 959–978. doi:10.1007/s10980-013-9868-y.

Myint, S. W., B. Zheng, E. Talen, C. Fan, S. Kaplan, A. Middel, M. Smith, H. P. Huang, and A. Brazel. 2015. "Does the Spatial Arrangement of Urban Landscape Matter? Examples of Urban Warming and Cooling in Phoenix and Las Vegas." *Ecosystem Health and Sustainability* 1 (4): 1–15. doi:10.1890/EHS14-0028.1.

Nastran, M., M. Kobal, and K. Eler. 2019. "Urban Heat Islands in Relation to Green Land Use in European Cities." *Urban*

Forestry & Urban Greening 37: 33–41. doi:10.1016/j.ufug.2018.01.008.

Oke, T. R. 1982. "The Energetic Basis of the Urban Heat Island." *Quarterly Journal of the Royal Meteorological Society* 108 (455): 1–24.

Oke, T. R., and H. A. Cleugh. 1987. "Urban Heat Storage Derived as Energy Balance Residuals." *Boundary-Layer Meteorology* 39 (3): 233–245. doi:10.1007/BF00116120.

Ord, J. K., and A. Getis. 1995. "Local Spatial Autocorrelation Statistics: Distributional Issues and an Application." *Geographical Analysis* 27 (4): 286–306. doi:10.1111/j.1538-4632.1995.tb00912.x.

Peng, J., P. Xie, Y. Liu, and J. Ma. 2016. "Urban Thermal Environment Dynamics and Associated Landscape Pattern Factors: A Case Study in the Beijing Metropolitan Region." *Remote Sensing of Environment* 173: 145–155. doi:10.1016/j.rse.2015.11.027.

Riitters, K. H., R. V. O'neill, C. T. Hunsaker, J. D. Wickham, D. H. Yankee, S. P. Timmins, K. B. Jones, and B. L. Jackson. 1995. "A Factor Analysis of Landscape Pattern and Structure Metrics." *Landscape Ecology* 10 (1): 23–39. doi:10.1007/BF00158551.

Rud, R., M. Shoshany, and V. Alchanatis. 2013. "Spatial–spectral Processing Strategies for Detection of Salinity Effects in Cauliflower, Aubergine and Kohlrabi." *Biosystems Engineering* 114 (4): 384–396. doi:10.1016/j.biosystemseng.2012.11.012.

Santamouris, M., N. Papanikolaou, I. Livada, I. Koronakis, C. Georgakis, A. Argiriou, and D. N. Assimakopoulos. 2001. "On the Impact of Urban Climate on the Energy Consumption of Buildings." *Solar Energy* 70 (3): 201–216. doi:10.1016/S0038-092X(00)00095-5.

Saura, S. 2004. "Effects of Remote Sensor Spatial Resolution and Data Aggregation on Selected Fragmentation Indices." *Landscape Ecology* 19 (2): 197–209. doi:10.1023/B:LAND.0000021724.60785.65.

Sobrino, J. A., J. C. Jiménez-Muñoz, and L. Paolini. 2004. "Land Surface Temperature Retrieval from LANDSAT TM 5." *Remote Sensing of Environment* 90 (4): 434–440. doi:10.1016/j.rse.2004.02.003.

Sobrino, J. A., J. C. Jiménez-Muñoz, G. Sòria, M. Romaguera, L. Guanter, J. Moreno, A. Plaza, and P. Martínez. 2008. "Land Surface Emissivity Retrieval from Different VNIR and TIR Sensors." *IEEE Transactions on Geoscience and Remote Sensing* 46 (2): 316–327. doi:10.1109/TGRS.2007.904834.

Song, J., S. Du, X. Feng, and L. Guo. 2014. "The Relationships between Landscape Compositions and Land Surface Temperature: Quantifying Their Resolution Sensitivity with Spatial Regression Models." *Landscape and Urban Planning* 123: 145–157. doi:10.1016/j.landurbplan.2013.11.014.

Songchitruksa, P., and X. Zeng. 2010. "Getis–Ord Spatial Statistics to Identify Hot Spots by Using Incident Management Data." *Transportation Research Record* 2165 (1): 42–51. doi:10.3141/2165-05.

Svensson, M. K., and I. Eliasson. 2002. "Diurnal Air Temperatures in Built-up Areas in Relation to Urban Planning." *Landscape and Urban Planning* 61 (1): 37–54. doi:10.1016/S0169-2046(02)00076-2.

Tomlinson, C. J., L. Chapman, J. E. Thornes, and C. J. Baker. 2011. "Including the Urban Heat Island in Spatial Heat Health Risk Assessment Strategies: A Case Study for Birmingham, UK." *International Journal of Health Geographics* 10 (1): 42. doi:10.1186/1476-072X-10-42.

Tran, D. X., F. Pla, P. Latorre-Carmona, S. W. Myint, M. Caetano, and H. V. Kieu. 2017. "Characterizing the Relationship between Land Use Land Cover Change and Land Surface Temperature." *ISPRS Journal of Photogrammetry and Remote Sensing* 124: 119–132. doi:10.1016/j.isprsjprs.2017.01.001.

Tucker, C. J. 1979. "Red and Photographic Infrared Linear Combinations for Monitoring Vegetation." *Remote Sensing of Environment* 8 (2): 127–150. doi:10.1016/0034-4257(79)90013-0.

Turner, M. G. 1989. "Landscape Ecology: The Effect of Pattern on Process." *Annual Review of Ecology and Systematics* 20 (1): 171–197. doi:10.1146/annurev.es.20.110189.001131.

Turner, M. G. 2005. "Landscape Ecology: What Is the State of the Science?" *Annual Review of Ecology, Evolution, and Systematics* 36 (1): 319–344. doi:10.1146/annurev.ecolsys.36.102003.152614.

Uuemaa, E., Ü. Mander, and R. Marja. 2013. "Trends in the Use of Landscape Spatial Metrics as Landscape Indicators: A Review." *Ecological Indicators* 28: 100–106. doi:10.1016/j.ecolind.2012.07.018.

Voogt, J. A., and T. R. Oke. 2003. "Thermal Remote Sensing of Urban Climates." *Remote Sensing of Environment* 86 (3): 370–384. doi:10.1016/S0034-4257(03)00079-8.

Wang, Y., and H. Akbari. 2016. "Analysis of Urban Heat Island Phenomenon and Mitigation Solutions Evaluation for Montreal." *Sustainable Cities and Society* 26: 438–446. doi:10.1016/j.scs.2016.04.015.

Weng, Q., D. Lu, and J. Schubring. 2004. "Estimation of Land Surface Temperature–vegetation Abundance Relationship for Urban Heat Island Studies." *Remote Sensing of Environment* 89 (4): 467–483. doi:10.1016/j.rse.2003.11.005.

Wolf, T., and G. McGregor. 2013. "The Development of a Heat Wave Vulnerability Index for London, United Kingdom." *Weather and Climate Extremes* 1: 59–68. doi:10.1016/j.wace.2013.07.004.

Wu, J. 2004. "Effects of Changing Scale on Landscape Pattern Analysis: Scaling Relations." *Landscape Ecology* 19 (2): 125–138. doi:10.1023/B:LAND.0000021711.40074.ae.

Wu, J., D. E. Jelinski, M. Luck, and P. T. Tueller. 2000. "Multiscale Analysis of Landscape Heterogeneity: Scale Variance and Pattern Metrics." *Geographic Information Sciences* 6 (1): 6–19. doi:10.1080/10824000009480529

Wu, J., W. Shen, W. Sun, and P. T. Tueller. 2002. "Empirical Patterns of the Effects of Changing Scale on Landscape Metrics." *Landscape Ecology* 17 (8): 761–782. doi:10.1023/A:1022995922992.

Wu, X., B. Li, M. Li, M. Guo, S. Zang, and S. Zhang. 2019. "Examining the Relationship between Spatial Configurations of Urban Impervious Surfaces and Land Surface Temperature." *Chinese Geographical Science* 29 (4): 568–578. doi:10.1007/s11769-019-1055-x.

Zhang, X., T. Zhong, X. Feng, and K. Wang. 2009. "Estimation of the Relationship between Vegetation Patches and Urban

Land Surface Temperature with Remote Sensing." *International Journal of Remote Sensing* 30 (8): 2105–2118. doi:10.1080/01431160802549252.

Zhang, Z., Y. Lv, and H. Pan. 2013. "Cooling and Humidifying Effect of Plant Communities in Subtropical Urban Parks." *Urban Forestry & Urban Greening* 12 (3): 323–329. doi:10.1016/j.ufug.2013.03.010.

Zheng, B., S. W. Myint, and C. Fan. 2014. "Spatial Configuration of Anthropogenic Land Cover Impacts on Urban Warming." *Landscape and Urban Planning* 130: 104–111. doi:10.1016/j.landurbplan.2014.07.001.

Zhibin, R., Z. Haifeng, H. Xingyuan, Z. Dan, and Y. Xingyang. 2015. "Estimation of the Relationship between Urban Vegetation Configuration and Land Surface Temperature with Remote Sensing." *Journal of the Indian Society of Remote Sensing* 43 (1): 89–100. doi:10.1007/s12524-014-0373-9.

Zhou, D., S. Zhao, S. Liu, L. Zhang, and C. Zhu. 2014. "Surface Urban Heat Island in China's 32 Major Cities: Spatial Patterns and Drivers." *Remote Sensing of Environment* 152: 51–61. doi:10.1016/j.rse.2014.05.017.

Zhou, W., G. Huang, and M. L. Cadenasso. 2011. "Does Spatial Configuration Matter? Understanding the Effects of Land Cover Pattern on Land Surface Temperature in Urban Landscapes." *Landscape and Urban Planning* 102 (1): 54–63. doi:10.1016/j.landurbplan.2011.03.009.

Zhou, X., and Y. C. Wang. 2011. "Dynamics of Land Surface Temperature in Response to Land-Use/Cover Change." *Geographical Research* 49 (1): 23–36. doi:10.1111/j.1745-5871.2010.00686.x.

ZIMSTAT. 2012. "Zimbabwe Population Census 2012" National Report. http://www.zimstat.co.zw/sites/default/files/img/National_Report.pdf